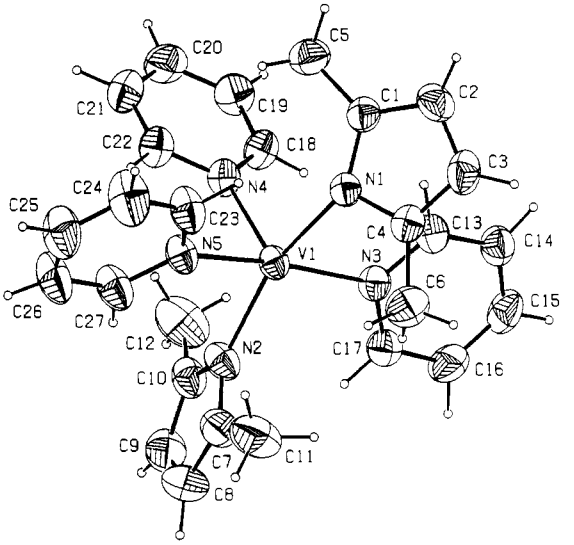

Figure 2. ORTEP plot of **9**. Thermal ellipsoids are drawn at the 50% probability level.

pyrazolyl). An unusual square-based-pyramidal coordination geometry has been observed in the case of the bulky pyrrolyl [2,5-$Me_2(C_4H_2N)$] derivative, which allowed the isolation of monomeric [2,5-$Me_2(C_4H_2N)]_2V(Py)_3$ (**9**) as deep red crystals after treatment with pyridine (Scheme IV).

The overall geometry of the vanadium atom in complex **9**, as demonstrated by X-ray analysis, may be described in terms of a distorted square-based pyramid, with two pyrrolyl groups, two molecules of pyridine, and the vanadium atom defining the basal plane and one additional molecule of pyridine positioned on the apical vertex. In contrast to the case of the isostructural d^4 Cr(II) derivative $(C_4H_4N)_2Cr(Py)_3$,[21] where the axial molecule of pyridine reaches a considerably longer Cr-N distance with respect to the other two basal pyridine molecules, the corresponding distance in complex **9** is slightly shorter [V1-N4 = 2.152 (2) Å versus V1-N3 = 2.233 (2) Å, V1-N5 = 2.211 (2) Å]. The V-N distances of the pyrrolyl groups are as expected [V1-N1 = 2.169 (2) Å, V1-N2 = 2.141 (2) Å] and compare well with those observed in the Cr(II) derivative.[21] The angle subtended at vanadium by the two nitrogen atoms of the two basal pyridine molecules is close to linear [N3-V1-N5 = 170.72 (7)°], while the angle formed by the two pyrrolyl groups is significantly smaller [N1-V1-N2 = 161.56 (7)°], as a probable result of the steric interaction of the two ortho methyl groups with the axial pyridine. In spite of the comparable V-N distances, the two pyrrolyl groups have a curiously different arrangement with respect to the vanadium atom. One ring is in fact coplanar with vanadium, while the second is significantly bent, the distance of vanadium from the ring plane being 0.823 (1) Å. So far, we are unable to explain this feature, since no other particular intramolecular contacts have been found.

The pyramidal geometry of **9** constitutes the first example where this type of geometry is observed in a d^3 system, using a simple monodentate nonmacrocyclic ligand. While a low-spin electronic configuration may be the factor that enforces this unusual coordination geometry in the isostructural Cr(II) $(pyrrolyl)_2Cr(pyridine)_3$[21] derivative, this can be excluded in the case of complex **9**, which showed the usual high-spin configuration (μ_{eff} = 3.65 μ_B), commonly observed in octahedral V(II) derivatives.

Acknowledgment. This work was supported by the Natural Sciences and Engineering Research Council of Canada (operating grant) and by the donors of the Petroleum Research Fund, administered by the American Chemical Society. The Nederlandse Organisatie voor Wetenschappelijk Onderzoek (NWO) is gratefully acknowledged for providing a visiting scholarship (J.J.H.E.) and for supporting part of the crystallographic work. X-ray data for **1** were kindly collected by A. J. M. Duisenberg.

Supplementary Material Available: Tables of crystal data, temperature factors, torsion angles, bond angles and distances, thermal parameters, and atomic positional parameters (15 pages); lists of structure factors for **1** and **9** (42 pages). Ordering information is given on any current masthead page.

(21) Edema, J. J. H.; Meetsma, A.; van Bolhuis, F.; Spek, A. L.; Smeets, W. J. J. *Inorg. Chem.* **1990**, *29*, 2147.

Contribution from the Department of Chemistry and the Center for Molecular Electronics, Center for Science and Technology, Syracuse University, Syracuse, New York 13244-4100

Small Heteroborane Cluster Systems. 3. Characterization, Deprotonation, and Transition-Metal Chemistry of the Small Phosphorus-Bridged Pentaborane(9) System (μ-Diphenylphosphino)pentaborane

Bruce H. Goodreau, Robert L. Ostrander, and James T. Spencer*

Received July 26, 1990

The complete spectroscopic characterization of the small phosphorus-bridged pentaborane(9) cluster (μ-diphenylphosphino)-pentaborane, [μ-$(C_6H_5)_2PB_5H_8$] (**1**), is reported. The MNDO calculated structure for **1** shows that the B-P-B interaction can be best described as consisting of two two-center-two-electron B-P bonding interactions. Indirect support for the involvement of the lone pair of electrons on the phosphorus in cage bonding is obtained from the failure of **1** to react with $[(CH_3CN)_3Mo(CO)_3]$ under forcing conditions. Compound **1** is readily and quantitatively bridge-deprotonated by the action of NaH to produce the corresponding anion, Na[(μ-$(C_6H_5)_2P)B_5H_7$] (**2**). Compound **2** reacts with 1 equiv of $[Fe(\eta^5\text{-}C_5H_5)(CO)_2I]$ to yield the iron complex [(μ-$(C_6H_5)_2P)B_5H_7Fe(\eta^5\text{-}C_5H_5)(CO)_2$] (**3**) in high yield as an air-stable, yellow solid. A single-crystal X-ray analysis of **3** shows that the structure consists of a highly distorted square pyramid of boron atoms in which the B(2)-H-B(3) bond in B_5H_9 has been subrogated by a B-P-B bridge and that the $[Fe(\eta^5\text{-}C_5H_5)(CO)_2]$ unit is σ-substituted for a terminal proton on B(4). The phosphorus atom exhibits a distorted tetrahedral geometry and is located 0.516 Å below the least-squares basal-B_4 plane. The B(2)-B(3) atomic distance of the B-P-B bridge was found to be 2.68 Å. The structure is formally derived from a two-electron reduction of a *nido*-pentaborane structure by the three-electron-donating phosphino unit to produce an *arachno*-pentaborane structure that is directly analogous to *arachno*-B_5H_{11}. Crystallographic data: space group $P2_1/n$ (No. 14), a = 10.989 (2) Å, b = 13.460 (4) Å, c = 14.454 (5) Å, $\alpha = \gamma = 90.00°$, β = 95.42 (2), V = 2128 (1) Å^3, Z = 4 molecules/cell.

Introduction

Insights into the synthesis, structure, and bonding of heteroborane polyhedral species provide important information on other classes of substituted main-group and organometallic polyhedra. As part of our continuing interest in the detailed chemistry of phosphorus-containing borane cluster compounds, we are exploring the synthetic and organometallic chemistry of the phosphinopentaborane class of heteroboranes.[1,2] Relatively few small

0020-1669/91/1330-2066$02.50/0 © 1991 American Chemical Society

phosphaborane cluster compounds have been reported,[1,3-8] and little is known of their organotransition-metal chemistry. Even fewer studies have thus far been reported in which the effect of the incorporated phosphorus atom on the small borane cage toward its reaction and organometallic chemistry has been probed.

In this paper, we report the first complete spectroscopic characterization and transition metal chemistry of the small bridged phosphinopentaborane cluster (μ-diphenylphosphino)-pentaborane (**1**). The molecular structure of the organometallic complex of **1** reported in this paper represents the first structural characterization of a phosphinopentaborane cluster. In addition, it is the first structural characterization of a pentaborane cage derivative in which both σ-metal coordination at a basal site and main-group heteroatom basal bridging have been observed. This structure provides confirmation of both the σ-coordination of the iron group to the cage and verification of the structural and bonding details of the phosphinopentaborane parent compound as predicted by spectroscopic analyses[1,3,5] and theoretical calculations.[2] The structure also provides support for the relatively unusual B(2) terminal substitution of the iron group postulated for the related $[B_5H_8(Fe(\eta^5\text{-}C_5H_5)(CO)_2)]$ complex reported by Gaines[9] and Greenwood.[10] Finally, this paper provides strong support for the proposed two two-center–two-electron bonding mode of the B–P–B bridging unit and provides direct information on the electronic effect of phosphorus substitution on small borane cages.

Experimental Section

Physical Measurements. Boron (^{11}B) NMR spectra were recorded on a Cryomagnetics spectrometer operating at 80.26 MHz. Spectra were recorded in 5-mm tubes in both the ^{1}H-coupled and decoupled modes and were externally referenced to BBr_3 at +40.0 ppm (positive chemical shifts indicate downfield resonances). Carbon (^{13}C) NMR spectra were obtained on a General Electric QE-300 spectrometer operating at 75.48 MHz. The spectrometer was operated in the FT mode while locked on the deuterium resonance of $CDCl_3$ or THF-d_8 solvent in 5-mm (o.d.) sample tubes. The reference was set relative to tetramethylsilane from the known chemical shifts of the solvent carbon atoms. Phosphorus (^{31}P) NMR spectra were obtained in 5-mm (o.d.) tubes on a Cryomagnetics spectrometer operating at 101.27 MHz. Chemical shifts were referenced to an external standard of 85% phosphoric acid sealed in a 1-mm capillary tube. Both proton broad-band-decoupled and -coupled spectra were routinely observed for each sample with a decoupling power of about 5 W. Proton (^{1}H) NMR spectra were obtained on a General Electric QE-300 spectrometer operating at 300.15 MHz. Spectra were recorded on samples dissolved in $CDCl_3$ or THF-d_8 in 5-mm (o.d.) tubes with chemical shifts referenced to internal tetramethylsilane, with a positive shift indicating a resonance at a lower applied field than that of the standard. Mass spectra were obtained on a Finnigan 4021 mass spectrometer using an ionization potential of between 11 and 30 eV. FT-IR spectra in the range 4000–400 cm^{-1} were measured on a Mattson Galaxy 2020 spectrometer and were referenced to the 1601.8-cm^{-1} band of polystyrene. All compounds were recorded as Nujol mulls sandwiched between NaCl plates. Elemental analyses were performed by the Schwarzkopf Microanalytical Laboratories, Woodside, NY.

Materials. All solvents were reagent grade or better. THF and pentane were distilled from sodium metal/benzophenone under a dry nitrogen atmosphere prior to use. Methylene chloride and hexane were used as received. All organic solvents, after appropriate drying, were degassed by repeated freeze–thaw cycles and finally stored in vacuo prior to use. Deuterated solvents were vacuum distilled onto 4-Å molecular sieves prior to use. Pentaborane(9) was taken directly from our laboratory stock. The $[Fe(\eta^5\text{-}C_5H_5)(CO)_2I]$ was prepared and purified by literature methods[11] from the reaction of $[Fe(\eta^5\text{-}C_5H_5)(CO)_2]_2$ with I_2. The $[Mo(CH_3CN)_3(CO)_3]$ was prepared from the reaction of $Mo(CO)_6$ with acetonitrile as previously reported.[12] The syntheses of several bridging phosphinopentaboranes, including $[\mu\text{-}(C_6H_5)_2PB_5H_8]$ (**1**), have been reported previously;[1,3] however, the procedure used for the synthesis of **1** in this work is significantly different from those reported earlier. A detailed account of the procedure used in this work for the synthesis of **1** is provided below. The following commercially available anhydrous chemicals were either used as received or purified by the method indicated and, where possible, were stored over 4-Å molecular sieves prior to use: $[Fe(\eta^5\text{-}C_5H_5)(CO)_2]_2$ (Strem), $Mo(CO)_6$ (Strem), iodine (Aldrich), $ClP(C_6H_5)_2$ (Aldrich), $ClP(O)(C_6H_5)_2$ (Aldrich), and sodium hydride (Aldrich) (the 80% suspension in mineral oil was washed several times with dry pentane and the washes decanted off to remove the mineral oil). Analytical thin-layer chromatography was conducted on 2.5 × 7.5 cm silica gel strips (1B-F, Baker) and conventional column chromatography was conducted using 4.0 × 20 cm columns packed with 230–400 mesh (ASTM) silica gel (EM Science).

Theoretical Calculations. The MNDO semiempirical calculations were performed by using MOPAC 5.0.[13] Parametrizations for the atoms were those reported in the literature.[14] Our initial parameters and standard procedures for the determination of the MNDO optimized structures for phosphinopentaboranes have been reported previously and were followed in the work reported here.[2] No unusual difficulties were encountered in the calculations.

$[(\mu\text{-}(C_6H_5)_2P)B_5H_8]$ (1). In a typical reaction, 0.53 g (22 mmol) of washed and dried NaH was placed in a round-bottom flask and evacuated to 5 × 10^{-5} Torr. Into this flask was condensed slightly less than 1 equiv of pentaborane(9), 1.3 g (20 mmol), and 50 mL of dry, degassed THF by using standard vacuum-line manipulations.[15] The reaction mixture was allowed to slowly warm to −50 °C with rapid stirring at which time vigorous hydrogen gas evolution was observed. After the bubbling had ceased, the resultant clear, colorless solution was frozen at −196 °C, and a solution containing 3.6 mL (20 mmol) of Ph_2PCl in 30 mL of dry degassed THF was added via syringe. The reaction mixture was then allowed to slowly warm to −78 °C and to stir at that temperature for 1 h. ^{11}B NMR analysis of the reaction mixture showed quantitative conversion of $Na[B_5H_8]$ to $[(\mu\text{-}(C_6H_5)_2P)B_5H_8]$ (**1**). The THF was removed in vacuo to yield a yellow, viscous oil. This oil was extracted with dry pentane (2 × 20 mL). ^{11}B NMR analysis showed that the extract contained pure **1**. The solvent was removed in vacuo to give a colorless, slightly air-sensitive oil obtained in 29% overall yield. Concentration of the reaction mixture appeared to cause an apparent decrease in the yield presumably due to product polymerization or decomposition in the condensed phase. Complete spectroscopic characterization of **1** is given in Tables I and II. No further purification was required, and the yield, as determined from ^{11}B NMR, was approximately quantitative.

Reaction of $Na[B_5H_8]$ with $(C_6H_5)_2PCl(O)$. A 20 mmol THF solution of $Na[B_5H_8]$ was prepared from the reaction of 1.3 g (20 mmol) of B_5H_9 with 0.48 g (20 mmol) of NaH in 20 mL of THF at −20 °C using standard techniques.[16,17] ^{11}B NMR characterization of the solution showed the presence of only $Na[B_5H_8]$. To this solution was added 4.7 g (20 mmol) of $(C_6H_5)_2PCl(O)$ in 20 mL of THF at −25 °C. When stirred for 30 min, the reaction mixture became yellow. ^{11}B NMR analysis of the reaction mixture showed only unreacted $Na[B_5H_8]$ and $Na[B_9H_{14}]$.[18] The reaction was allowed to stir for an additional 24 h at −25 °C, after which time a ^{11}B NMR analysis of the reaction mixture showed only $B_5H_8^-$ decomposition products (primarily $B_9H_{14}^-$ and B_5H_9).

Reaction of $[(\mu\text{-}(C_6H_5)_2P)B_5H_8]$ (1) with $[(CH_3CN)_3Mo(CO)_3]$. Under a dry nitrogen atmosphere, 1.23 g (5.0 mmol) of **1** in 100 mL of dry, degassed THF was added to 0.50 g (1.6 mmol) of $[(CH_3CN)_3Mo(CO)_3]$ in 200 mL of THF. The reaction mixture was stirred for 8 h at room temperature. ^{11}B and ^{31}P analysis of the reaction showed no signs of

(1) Part 2: Miller, R. W.; Donaghy, K. J.; Spencer, J. T. *Organometallics*, in press.
(2) Glass, J. A., Jr.; Whelan, T. A.; Spencer, J. T. *Organometallics*, in press.
(3) Mishra, I. B.; Burg, A. B. *Inorg.* Chem. **1972**, *11*, 664.
(4) Burg, A. B.; Heinen, H. *Inorg. Chem.* **1968**, *7*, 1021.
(5) Coons, D. E.; Gaines, D. F. *Inorg. Chem.* **1987**, *26*, 1985.
(6) Haubold, W.; Keller, W.; Sawitzki, G. *Angew. Chem., Int. Ed. Engl.* **1988**, *27*, 925.
(7) Burg, A. B. *Inorg. Chem.* **1973**, *12*, 3017.
(8) Wood, G. L.; Duesler, E. N.; Narula, C. K.; Paine, R. T.; Noth, H. *J. Chem. Soc., Chem. Commun.* **1987**, 496.
(9) Fischer, M. B.; Gaines, D. F.; Ulman, J. A. *J. Organomet. Chem.* **1982**, *231*, 55.
(10) Greenwood, N. N.; Kennedy, J. D.; Savory, C. G.; Staves, J.; Trigwell, K. R. *J. Chem. Soc., Dalton Trans.* **1978**, 237.
(11) King, R. B. *Organometallic Synthesis*; Academic Press: New York, 1965; Vol. 1, p 175.
(12) Tate, D. P.; Knipple, W. R.; Augl, J. M. *Inorg. Chem.* **1962**, *1*, 433.
(13) Stewart, J. J. P.; Seiler, F. J. Quantum Chemistry Program Exchange, Program No. 549.
(14) Parameterizations used for the MNDO calculations were as follows: (a) (boron) Dewar, M. J. S.; McKee, M. L. *J. Am. Chem. Soc.* **1977**, *99*, 5231. (b) (hydrogen, carbon, and oxygen) Dewar, M. J. S.; Theil, W. *J. Am. Chem. Soc.* **1977**, *99*, 4899. (c) (phosphorus) Dewar, M. J. S.; McKee, M. L. Rzepa, H. S. *J. Am. Chem. Soc.* **1978**, *100*, 3607.
(15) Shriver, D. F.; Drezdzon, M. A. *The Manipulation of Air-Sensitive Compounds*; Wiley-Interscience: New York, 1986.
(16) Fessler, M. E.; Whelan, T.; Spencer, J. T.; Grimes, R. N. *J. Am. Chem. Soc.* **1987**, *109*, 7416.
(17) Gaines, D. F.; Iorns, T. V. *J. Am. Chem. Soc.* **1967**, *89*, 3375.
(18) Wermer, J. R.; Shore, S. G. *Advances in Boron and the Boranes*; VCH Publishers: New York, 1988; pp 15–19.

Table I. NMR Data for Phosphinopentaborane Systems

compd	^{11}B data[a]	^{1}H data[b]	^{13}C{^{1}H} data[b]	^{31}P data[c]	ref
$[Ph_2PB_5H_8]$ (1)[d]	−0.5 (d, B(4,5), J_{BH} = 164 Hz), −22.7 (t, B(2,3), J_{BH} = 110 Hz J_{BP} = 94 Hz), −45.6 (d, B(1), J_{BH} = 153 Hz)	−1.72 (br s, 3 H, bridging H), 7.40 (m, 8 H, *o,m*-C_6H_5), 7.79 (m, 2 H, *p*-C_6H_5)	130.41 (d, *o*-C_6H_5, J_{PC} = 12.3 Hz), 133.29 (d, *o*-C_6H_5, J_{PC} = 8.5 Hz), 128.65 (d, *m*-C_6H_5, J_{PC} = 11.2 Hz), 128.94 (d, *m*-C_6H_5, J_{PC} = 9.6 Hz), 130.31 (d, *p*-C_6H_5, J_{PC} = 2.4 Hz), 130.48 (d, *p*-C_6H_5, J_{PC} = 4.5 Hz), 132.94 (d, *i*-C_6H_5, J_{PC} = 17.9 Hz), 136.07 (d, *i*-C_6H_5, J_{PC} = 15.7 Hz)	−52.3 (br s)	this work[e]
$Na[Ph_2PB_5H_7]$ (2)[f]	−3.0 (d, B(4,5), J_{BH} = 185 Hz), −23.5 (t, B(2,3), J_{BH} = 134 Hz, J_{BP} = 59.7 Hz), −48.0 (d, B(1), J_{BH} = 172 Hz)	−2.74 (br s, 3 H, bridging H), −0.96 (q, 5 H, terminal BH J_{BH} = 136.3 Hz), 7.16 (m, 8 H, *o,m*-C_6H_5), 7.87 (m, 2 H, *p*-C_6H_5)	131.01 (d, *o*-C_6H_5, J_{PC} = 11.6 Hz), 134.43 (d, *o*-C_6H_5, J_{PC} = 7.1 Hz), 127.81 (d, *m*-C_6H_5, J_{PC} = 10.9 Hz), 128.12 (d, *m*-C_6H_5, J_{PC} = 6.4 Hz), 128.01 (d, *p*-C_6H_5, J_{PC}, unres), 128.06 (d, *p*-C_6H_5, J_{PC} = 3.0 Hz)[g]	−38.9 (br s)	this work
$[Cp(CO)_2Fe(B_5H_7PPh_2)]$ (3)[f,h]	23.3 (s, B(4)), 1.4 (d, B(5), J_{BH} = 166 Hz), −23.6 (m, B(3), J_{BH} = unres J_{BP} = 83 Hz), −24.9 (m, B(2), J_{BH} = unres J_{BP} = 83 Hz), −37.6 (d, B(1), J_{BH} = 155 Hz)	−1.34 (br s, 3 H, bridging H), 4.83 (s, 5 H, C_5H_5), 7.41 (br, 8 H, *o,m*-C_6H_5), 7.79 (br, 2 H, *p*-C_6H_5)	85.78 (s, C_5H_5), 131.34 (d, *o*-C_6H_5, J_{PC} = 12.7 Hz), 134.13 (d, *o*-C_6H_5, J_{PC} = 8.3 Hz), 129.45 (d, *m*-C_6H_5, J_{PC} = 11.5 Hz), 129.64 (d, *m*-C_6H_5, J_{PC} = 9.2 Hz), 130.74 (d, *p*-C_6H_5, J_{PC} = 2.1 Hz), 130.89 (d, *p*-C_6H_5, J_{PC} unres), 138.88 (d, *i*-C_6H_5, J_{PC} = 13.4 Hz),[i] 216.64 (s, *C*O), 216.88 (s, *C*O)	−50.4 (br s)	this work
$[Cp(CO)_2FeB_5H_8]$ (4)[j]	7.9 (s, B(2)), −10.6 (d, B(3,4), J_{BH} = 150 Hz), −14.3 (d, B(5), J_{BH} = 160 Hz), −48.5 (d, B(1), J_{BH} = 170 Hz)	−2.7 (m, 3 H, terminal H, J_{BH} = 156 Hz), −0.9 (m, 1 H, terminal H, J_{BH} = 168 Hz), 0.8 (br s, 2 H, bridging H), 1.9 (br s, 2 H, bridging H), 4.95 (br s, 5 H, C_5H_5)			5

[a] Relative to BBr_3 (40.0 ppm). Abbreviations: s = singlet, d = doublet, t = pseudotriplet (overlapping doublet of doublets), q = quartet, m = multiplet, unres = unresolved coupling, *o* = ortho, *m* = meta, *p* = para, *i* = ipso, br = broad. [b] Relative to TMS (0.0 ppm). [c] Relative to 85% H_3PO_4 (0.0 ppm). [d] In $CDCl_3$. [e] ^{11}B data reported in ref 6 were as follows (positive values are reported upfield from $(MeO)_3B$): δ 21 (d, B(4,5), J_{BH} = 166 Hz), 44 (d, B(2,3), J_{BH} = 156 Hz), 66 (d, B(1), J_{BH} = 200 Hz). [f] In THF-d_8. [g] Neither ipso carbon of the C_6H_5 group was observed. [h] Sine multiplication resolution enhancement applied to the FID in the ^{11}B NMR analysis.[18] [i] One ipso carbon of the C_6H_5 group was not observed. [j] In C_6D_6. In the numbering scheme used in ref 5, the $[Fe(\eta^5\text{-}C_5H_5)(CO)_2]$ unit is attached to the B_5 cage at B(2).

reaction. The reaction mixture was then refluxed for an additional 8 h. ^{11}B and ^{31}P analysis of the solution again showed no signs of reaction.

$Na[(\mu\text{-}(C_6H_5)_2P)B_5H_7]$ (2). A solution containing 4.1 g (16.5 mmol) of **1** in 20 mL of dry THF was syringed into a 250-mL round-bottom flask that contained 0.48 g (20 mmol) of NaH under a dry nitrogen atmosphere at −196 °C. The contents of the flask were frozen at −196 °C and the flask was evacuated to 5 × 10^{-5} Torr. The reaction was allowed to warm slowly to −50 °C with rapid stirring. Vigorous gas evolution was observed upon warming. The gas evolution was monitored and showed quantitative formation of hydrogen gas within an hour. Once the rate of the bubbling had significantly slowed, the flask was warmed to 0 °C and stirred for an additional hour. The clear yellow reaction solution was decanted from the small amount of unreacted NaH that remained in the flask. ^{11}B NMR analysis of this yellow solution indicated complete conversion of **1** to $Na[(\mu\text{-}(C_6H_5)_2P)B_5H_7]$ (**2**). The THF solvent was removed in vacuo to obtain an air-sensitive, yellow solid. ^{11}B and ^{31}P NMR showed the solid to be pure **2**. No further purification was required. Complete spectroscopic characterization of **2** is given in Tables I and II.

The yellow solid, **2** obtained above can be converted to a colorless solid by extended vacuum pumping at room temperature. The addition of THF to the colorless solid regenerates the yellow solution, which in turn gives back the yellow solid on removal of solvent. This process is apparently a reversible coordination of THF sovlent to **2**. Gentle heating of compound **2** resulted in its decomposition into **1** and an unidentified nonvolatile B–P species.

$[(\mu\text{-}(C_6H_5)_2P)B_5H_7Fe(\eta^5\text{-}C_5H_5)(CO)_2]$ (3). Under a dry nitrogen atmosphere, a freshly prepared solution of 3.93 g (14.6 mmol) of **2** in 20 mL of dry THF (prepared from the reaction of 0.48 g (20 mmol) of dry NaH with 3.61 g (14.6 mmol) of **1**) was syringed into a flask that contained 4.56 g (15.0 mmol) of $[Fe(\eta^5\text{-}C_5H_5)(CO)_2I]$ at 0 °C. The solution rapidly became dark brown and was allowed to warm slowly to room temperature and then to stir for 1 h. ^{11}B analysis of the reaction mixture show a quantitative conversion to product. The solvent was removed in vacuo to give a brown, air-stable solid. The solid was extracted with methylene chloride, the solution concentrated and then chromatographed on a 4 × 20 cm silica gel column, which was eluted with a 50% methylene chloride in hexane solution. First to elute was a yellow band, which contained the pure $[(\mu\text{-}(C_6H_5)_2P)B_5H_7Fe(\eta^5\text{-}C_5H_5)(CO)_2]$ (**3**) (R_f = 0.82). Removal of sovlent provided **3** as a yellow, air-stable solid in 22% isolated yield. Complete spectroscopic characterization of **3** is given in Tables I and II. Anal. Calcd (found) for $C_{19}H_{22}B_5FeO_2P$: C, 53.90 (54.27); H, 5.20 (5.23); B, 12.77 (12.76); Fe, 13.24 (12.74); P, 7.33 (6.87).

X-ray Crystallography. A cubic yellow crystal of $[(\mu\text{-}(C_6H_5)_2P)B_5H_7Fe(\eta^5\text{-}C_5H_5)(CO)_2]$ (**3**), with approximate dimensions of 0.55 × 0.30 × 0.30 mm, was grown from a saturated 30% methylene chloride in pentane solution by slow solvent evaporation. The crystal was mounted in a 0.3-mm Lindemann capillary tube and sealed under an inert atmosphere. All measurements were made on a Rigaku AFC5S diffractometer using graphite-monochromated Mo Kα radiation (λ = 0.71073 Å). Cell constants and an orientation matrix for the data collection were obtained from a least-squares refinement using 25 centered high-angle reflections in the range 39.13° < 2θ < 43.50°. On the basis of the systematic absences of *h*0*l*, $h + l \neq 2n$, and 0*k*0, $k \neq 2n$, and the successful structural solution, the space group was uniquely determined to be $P2_1/n$. Data were collected at room temperature by using a ω-2θ scan technique to a maximum 2θ value of 60.0°. Three reference reflections were monitored every 100 reflections during data collection with no intensity loss observed during the collection. Crys-

Table II. Infrared and Mass Spectral Data for Phosphinopentaborane Systems

compd	IR data,[a] cm^{-1}	mass spectral data[b]	ref
$[Cp(CO)_2FeI]$	2037 (s, ν_{CO}), 1978 (s, ν_{CO})		10[c]
$[Ph_2PB_5H_8]$ (1)	3053 (m, ν_{ArCH}), 2586 (s, ν_{BH}), 2533 (s, ν_{BH}), 2382 (s, ν_{BH}), 1951 (w), 1882 (w), 1805 (w), 1757 (w), 1091 (m), 1049 (w), 1008 (w), 959 (m), 904 (m), 855 (m), 758 (m), 730 (m), 675 (s)	249 (found 9.5, calcd 11.0; P^+ envelope), 248 (found 82.3, calcd 87.9; P^+ envelope, $^{12}C_{12}{}^1H_{18}{}^{11}B_5{}^{31}P$), 247 (found 100.0, calcd 100.0; P^+ envelope), 246 (found 47.3, calcd 48.4; P^+ envelope), 245 (found 13.9, calcd 11.9; P^+ envelope), 244 (found 1.7, calcd 1.5; P^+ envelope), 186 (1.7, $HP(C_6H_5)_2$), 171 (1.2, $HP(C_6H_5)(B_5H_8)$)	this work
$Na[Ph_2PB_5H_7]$ (2)	3055 (w, ν_{ArCH}), 2381 (s, ν_{BH}), 1252 (w), 796 (w), 738 (w), 687 (w)		this work
$[Cp(CO)_2Fe(B_5H_7PPh_2)]$ (3)	2576 (m, ν_{BH}), 2513 (s, ν_{BH}), 1990 (vs, ν_{CO}), 1934 (vs, ν_{CO}), 1766 (m), 1462 (m), 1383 (m), 1259 (s), 1093 (s), 1020 (s), 796 (s), 687 (m), 644 (w), 586 (m), 499 (w)	426 (found 2.4, calcd 2.7; P^+ envelope), 425 (found 18.2, calcd 20.0; P^+ envelope), 424 (found 91.5, calcd 93.1; P^+ envelope, $^{12}C_{19}{}^1H_{22}{}^{11}B_5{}^{56}Fe^{16}O_2{}^{31}P$), 423 (found 100.0, calcd 100.0; P^+ envelope), 422 (found 53.4, calcd 52.4; P^+ envelope), 421 (found 17.7, calcd 17.5; P^+ envelope), 420 (found 4.3, calcd 4.2; P^+ envelope), 395 (31.6, $P^+ - CO$), 367 (100.0, $P^+ - 2CO$)	this work
$[Cp(CO)_2Fe(B_5H_8)]$[d] (4)	2575 (s, ν_{BH}), 2012 (s, ν_{CO}), 1956 (s, ν_{CO}), 2575 (s, Nujol), 2005 (s, Nujol), 1946 (s, Nujol), 1805 (w, Nujol), 1779 (w, Nujol)	240 (P^+ envelope, $^{12}C_7{}^1H_{13}{}^{11}B_5{}^{56}Fe^{16}O_2$), 239 ($P^+$ envelope), 238 (P^+ envelope), 184 ($Fe(B_5H_8(\eta^5\text{-}C_5H_5)$ envelope, $^{12}C_5{}^1H_{13}{}^{11}B_5{}^{56}Fe$), 183 ($Fe(B_5H_8)(\eta^5\text{-}C_5H_5)$ envelope), 182 ($Fe(B_5H_8)(\eta^5\text{-}C_5H_5)$ envelope), 180 ($Fe(B_5H_8)(\eta^5\text{-}C_5H_5)$ envelope)	5

[a] NaCl plates (unless otherwise indicated). Abbreviations: vs = very strong, s = strong; m = medium; w = weak; sh = shoulder; br = broad. [b] Relative intensities are given with the largest peak in the envelope normalized to 100.0%. The calculated values are based on natural isotopic abundances, which are normalized to the most intense peak in the envelope. [c] Values reported are from our measurements. [d] FT-IR in CCl_4.

Table III. Crystallographic Data for $[(C_6H_5)_2PB_5H_7Fe(\eta^5\text{-}C_5H_5)(CO)_2]$ (3)

chem formula	$C_{19}H_{22}B_5FeO_2P$	diffractometer	Rigaku AFC5S
fw	423.25	ρ_{calcd}, g cm^{-3}	1.321
cryst syst	monoclinic	μ, cm^{-1}	7.92
space group	$P2_1/n$ (No. 14)	transm coeff	
temp, K	298	Ψ	0.9788–1.0000
cell dimens		Ψ_{av}	0.9885
(at 298 K)		R, %	3.9
a, Å	10.989 (2)	R_w, %	3.9
b, Å	13.460 (4)	tot. no. of reflcns	6447
c, Å	14.454 (5)	no. of reflcns with $I > 3\sigma(I)$	3186
α, deg	90.00		
β, deg	95.42 (2)	no. of variables	341
γ, deg	90.00	$2\theta_{max}$, deg	60.0
V, Å^3	2128 (1)	goodness of fit	1.31
Z, molecules/cell	4	max shift/error in final cycle	0.02
λ(Mo Kα)	0.71073		

tallographic data for this compound are presented in Table III.

Data reduction of the 6750 measured reflections resulted in 6447 unique reflections (R_{int} = 0.022). After the application of corrections for Lorentz and polarization effects, 3186 independent reflections with $I > 3\sigma(I)$ in the range $2\theta < 60°$ were obtained, which were used for the structure refinement (reflection/parameter = 9.34). Azimuthal scans of several reflections indicated that an absorption correction was not required. The position of the iron atom was determined from a Patterson synthesis, and the remaining non-hydrogen atoms were located by application of direct methods to generate a trial structure.[19,20] The non-hydrogen atoms refined anisotropically. The boron cage hydrogen atoms were then located on a difference map and were refined isotropically. All other hydrogen atoms were calculated and refined isotropically. The final cycle of a full-matrix least squares refinement converged with $R = \sum||F_o| - |F_c||/\sum|F_o| = 0.039$ and $R_w = [(\sum w(|F_o| - |F_c|)^2/\sum w(F_o^2)^2)]^{1/2} = 0.039$. The function minimized was $\sum w(|F_o| - |F_c|)^2$ (where $w = 4F_o^2/s^2(F_o^2)$, $s^2(F_o^2) = [S^2(C + R^2B) + (pF_o^2)^2](Lp)^2$).[23] Plots of $\sum w(|F_o| - |F_c|)^2$ versus $|F_o|$, reflection order in data collection, $(\sin\theta)/\lambda$, and various classes of indicies showed no unusual trends. The weighting scheme was based on counting statistics and included a factor (p = 0.03) to downweight intense reflections. Atomic scattering factors were from Cromer and Waber.[21] Terms for anomolous scattering were included in F_c[22] and used the values for $\Delta f'$ and $\Delta f''$ previously reported.[23] The

Table IV. Positional Parameters and B(eq) for $[(C_6H_5)_2PB_5H_7Fe(\eta^5\text{-}C_5H_5)(CO)_2]$ (3)

atom	x	y	z	B(eq), Å^2
Fe	0.12253 (3)	0.04699 (3)	0.21039 (3)	2.96 (2)
P	0.57765 (6)	0.01194 (5)	0.32070 (5)	2.54 (3)
O(1)	0.1865 (3)	0.2529 (2)	0.2404 (2)	7.1 (2)
O(2)	0.1354 (2)	0.0464 (2)	0.0114 (2)	6.4 (1)
C(1)	0.1627 (3)	0.1701 (3)	0.2269 (3)	4.4 (2)
C(2)	0.1306 (3)	0.0479 (3)	0.0909 (2)	4.1 (1)
C(3)	0.0800 (4)	0.0019 (3)	0.3414 (3)	5.0 (2)
C(4)	−0.0171 (3)	0.0568 (3)	0.2981 (3)	5.3 (2)
C(5)	−0.0613 (3)	0.0085 (4)	0.2184 (3)	5.5 (2)
C(6)	0.0073 (5)	−0.0763 (4)	0.2106 (3)	6.0 (2)
C(7)	0.0942 (4)	−0.0805 (3)	0.2868 (3)	5.4 (2)
C(8)	0.6419 (2)	−0.0948 (2)	0.3861 (2)	2.7 (1)
C(9)	0.5649 (3)	−0.1666 (3)	0.4150 (2)	4.3 (2)
C(10)	0.6112 (5)	−0.2516 (3)	0.4595 (3)	6.2 (2)
C(11)	0.7345 (5)	−0.2658 (3)	0.4736 (3)	6.3 (2)
C(12)	0.8120 (4)	−0.1957 (3)	0.4456 (3)	5.6 (2)
C(13)	0.7673 (3)	−0.1108 (3)	0.4021 (3)	4.2 (2)
C(14)	0.6713 (2)	0.1169 (2)	0.3623 (2)	2.6 (1)
C(15)	0.7010 (3)	0.1924 (2)	0.3032 (2)	3.4 (1)
C(16)	0.7695 (3)	0.2731 (3)	0.3364 (3)	4.2 (2)
C(17)	0.8095 (3)	0.2799 (3)	0.4280 (3)	4.4 (2)
C(18)	0.7816 (4)	0.2059 (3)	0.4877 (3)	4.8 (2)
C(19)	0.7125 (3)	0.1247 (2)	0.4556 (2)	4.0 (2)
B(1)	0.4311 (3)	0.0931 (3)	0.2033 (2)	2.7 (1)
B(2)	0.5604 (3)	0.0132 (3)	0.1888 (2)	2.8 (1)
B(3)	0.4105 (3)	0.0500 (3)	0.3209 (2)	2.9 (1)
B(4)	0.3076 (3)	0.0233 (2)	0.2193 (2)	2.7 (1)
B(5)	0.4085 (3)	−0.0080 (3)	0.1364 (2)	3.2 (1)
H(1B)	0.424 (2)	0.172 (2)	0.181 (2)	3.6 (6)
H(2B)	0.633 (3)	0.026 (2)	0.145 (2)	3.9 (7)
H(3B)	0.378 (2)	0.091 (2)	0.377 (2)	3.8 (7)
H(5B)	0.391 (2)	−0.012 (2)	0.065 (2)	3.1 (6)
H(6B)	0.510 (3)	−0.064 (2)	0.169 (2)	3.9 (7)
H(7B)	0.344 (3)	−0.026 (2)	0.307 (2)	4.2 (7)
H(8B)	0.339 (3)	−0.063 (2)	0.176 (2)	4.8 (7)

(19) Calbrese, J. C. PHASE—Patterson Heavy Atom Solution Extractor. Ph.D. Thesis, University of Wisconsin—Madison, 1972.
(20) Beurskens, P. T. DIRDIF: Direct Methods for Difference Structures. Technical Report 1984/1; Crystallography Laboratory: Toernooiveld, 6525 Ed. Nijmegen, Netherlands.
(21) Cromer, D. T.; Waber, J. T. *International Tables for X-ray Crystallography*; Kynoch: Birmingham, England, 1974; Vol. IV, Table 2.2A.

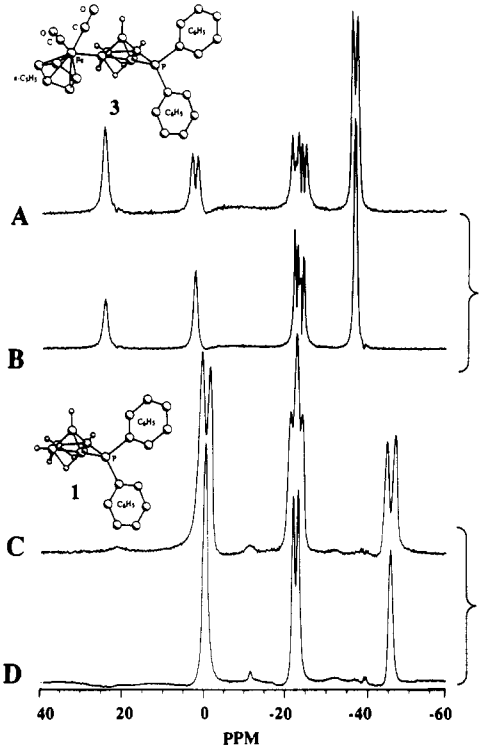

Figure 1. 80-MHz ^{11}B NMR spectra for $[(\mu\text{-}P(C_6H_5)_2)B_5H_8]$ (**1**) and $[(4\text{-}(Fe(\eta^5\text{-}C_5H_5)(CO)_2))B_5H_7(2\text{-}\mu\text{-}P(C_6H_5)_2)]$ (**3**) in $CDCl_3$ relative to BBr_3 (40.0 ppm): (a) $^{11}B\{^1H\}$ spectrum of **3**; (b) ^{11}B (^1H-coupled) spectrum of **3**; (c) $^{11}B\{^1H\}$ spectrum of **1**; (d) ^{11}B (^1H-coupled) spectrum of **1**. The spectra shown in parts a and b for compound **3** are "sine resolution enhanced" spectra. While this technique is very effective in resolving ^{11}B spectra, it does not provide accurate integrations. The integrations reported for all compounds were obtained without the use of this technique.

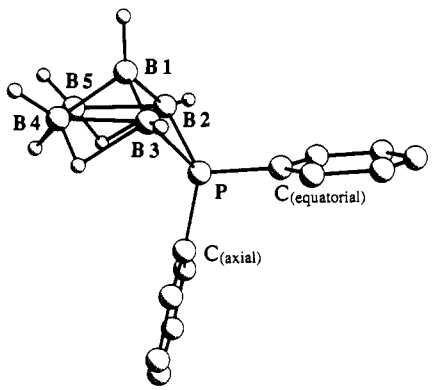

Figure 2. MNDO calculated minimum energy geometry for compound **1**. Hydrogen atoms on the phenyl groups have been omitted for clarity.

maximum and minimum peaks on the final difference Fourier map corresponded to 0.34 and −0.23 e/Å^3, respectively. Final atom coordinates and B(eq) are given in Table IV. A full tabular presentation of crystallographic data, including complete tables of intramolecular and intermolecular bond distances and angles, anisotropic thermal parameters, all atom coordinates including calculated and refined hydrogen atoms, and observed and calculated structure factors is available as supplementary material.

The final structure was plotted by using the TEXSAN[24a] graphics programs including PLUTO[24b] and ORTEP.[25] Figures 3 and 4 show the molecular and stereopair drawings of **3** with the atom-labeling scheme indicated. Selected bond angles and bond lengths are given in Tables V and VI, respectively. Selected least-squares planes and the dihedral angles between these planes are given in Tables VII.

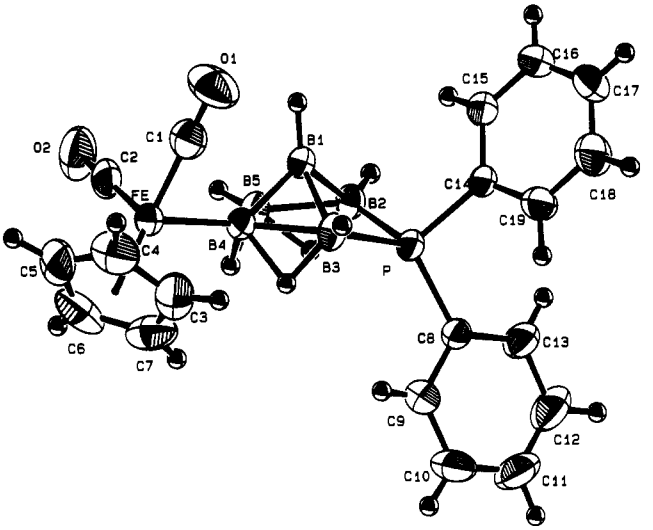

Figure 3. ORTEP drawing of **3** showing the atomic numbering scheme. The thermal elipsoids are drawn at the 50% probability level.

Table V. Selected Intramolecular Bond Angles (deg) for $[(C_6H_5)_2PB_5H_7Fe(\eta^5\text{-}C_5H_5)(CO)_2]$ (**3**)[a]

C(1)-Fe-C(2)	95.4 (2)	C(6)-Fe-B(4)	118.3 (2)
C(1)-Fe-C(3)	103.3 (2)	C(7)-Fe-B(4)	92.1 (2)
C(1)-Fe-C(4)	92.8 (2)	C(8)-P-C(14)	105.2 (1)
C(1)-Fe-C(5)	117.6 (2)	C(8)-P-B(2)	121.6 (1)
C(1)-Fe-C(6)	155.6 (2)	C(8)-P-B(3)	122.5 (1)
C(1)-Fe-C(7)	140.2 (2)	C(14)-P-B(2)	109.0 (1)
C(1)-Fe-B(4)	84.4 (1)	C(14)-P-B(3)	107.8 (1)
C(2)-Fe-C(3)	160.4 (2)	B(2)-P-B(3)	89.7 (1)
C(2)-Fe-C(4)	135.5 (2)	Fe-C(1)-O(1)	177.4 (3)
C(2)-Fe-C(5)	101.3 (2)	Fe-C(2)-O(2)	178.6 (3)
C(2)-Fe-C(6)	95.4 (2)	Fe-C(3)-C(4)	70.5 (2)
C(2)-Fe-C(7)	123.9 (2)	Fe-C(3)-C(7)	70.6 (2)
C(2)-Fe-B(4)	85.4 (1)	C(4)-C(3)-C(7)	107.0 (4)
C(3)-Fe-C(4)	39.1 (2)	Fe-C(4)-C(3)	70.4 (2)
C(3)-Fe-C(5)	65.1 (2)	Fe-C(4)-C(5)	71.4 (2)
C(3)-Fe-C(6)	65.1 (2)	C(3)-C(4)-C(5)	108.7 (4)
C(3)-Fe-C(7)	38.7 (2)	Fe-C(5)-C(4)	70.3 (2)
C(3)-Fe-B(4)	101.8 (1)	Fe-C(5)-C(6)	70.3 (2)
C(4)-Fe-C(5)	38.2 (2)	C(4)-C(5)-C(6)	108.0 (4)
C(4)-Fe-C(6)	64.4 (2)	Fe-C(6)-C(5)	71.2 (2)
C(4)-Fe-C(7)	64.7 (2)	Fe-C(6)-C(7)	70.3 (2)
C(4)-Fe-B(4)	139.0 (2)	C(5)-C(6)-C(7)	107.9 (4)
C(5)-Fe-C(6)	38.5 (2)	Fe-C(7)-C(3)	70.8 (2)
C(5)-Fe-C(7)	64.8 (2)	Fe-C(7)-C(6)	70.8 (2)
C(5)-Fe-B(4)	155.8 (2)	C(3)-C(7)-C(6)	108.4 (4)
C(6)-Fe-C(7)	38.9 (2)	P-C(8)-C(9)	119.4 (2)
P-C(8)-C(9)	119.4 (2)	P-C(14)-C(15)	121.7 (2)
P-C(8)-C(13)	122.4 (2)	P-C(14)-C(19)	120.2 (2)
C(9)-C(8)-C(13)	117.9 (3)	C(15)-C(14)-C(19)	118.0 (3)
C(8)-C(9)-C(10)	120.8 (4)	C(14)-C(15)-C(16)	120.8 (3)
C(9)-C(10)-C(11)	120.0 (4)	C(15)-C(16)-C(17)	120.5 (3)
C(10)-C(11)-C(12)	120.0 (4)	C(16)-C(17)-C(18)	119.6 (3)
B(2)-B(1)-B(5)	61.7 (2)	C(17)-C(18)-C(19)	120.7 (4)
B(3)-B(1)-B(4)	61.5 (2)	C(14)-C(19)-C(18)	120.3 (3)
B(3)-B(1)-B(5)	104.7 (3)	B(2)-B(1)-B(3)	94.9 (2)
B(4)-B(1)-B(5)	63.2 (2)	B(2)-B(1)-B(4)	109.6 (2)
P-B(2)-B(1)	83.9 (2)	Fe-B(4)-B(1)	135.4 (2)
P-B(2)-B(5)	115.1 (2)	Fe-B(4)-B(3)	124.2 (2)
B(1)-B(2)-B(5)	55.4 (2)	Fe-B(4)-B(5)	132.2 (2)
P-B(3)-B(1)	83.1 (2)	B(1)-B(4)-B(3)	63.2 (2)
P-B(3)-B(4)	118.4 (2)	B(1)-B(4)-B(5)	58.1 (2)
B(1)-B(3)-B(4)	55.2 (2)	B(3)-B(4)-B(5)	102.5 (2)
C(11)-C(12)-C(13)	120.5 (4)	B(1)-B(5)-B(2)	62.9 (2)
C(8)-C(13)-C(12)	120.7 (4)	B(1)-B(5)-B(4)	58.7 (2)
		B(2)-B(5)-B(4)	107.2 (2)

[a] Estimated standard deviations in the least significant figure are given in parentheses.

(22) Ibers, J. A.; Hamilton, J. T. *Acta Crystallogr.* **1964**, *17*, 781.
(23) Cromer, D. T.; Waber, J. T. *International Tables for X-ray Crystallography*; Kynoch: Birmingham, England, 1974; Vol. IV, Table 2.3.1.
(24) (a) TEXSAN—Texray Structure Analysis Package. Molecular Structure Corp. 1985. (b) Motherwell, S.; Clegg, W. PLUTO. Program for plotting molecular and crystal structures. University of Cambridge, England, 1978.
(25) Johnson, C. K. ORTEPII. Report ORNL-5138; Oak Ridge National Laboratory: Oak Ridge, TN, 1976.

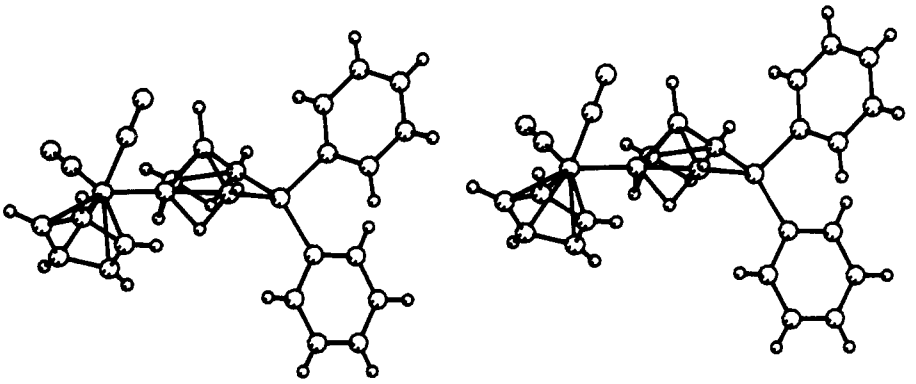

Figure 4. Stereopair PLUTO drawing of $[(C_6H_5)_2PB_5H_7Fe(\eta^5\text{-}C_5H_5)(CO)_2]$ (3).

Table VI. Selected Intramolecular Bond Distances (Å) for $[(C_6H_5)_2PB_5H_7Fe(\eta^5\text{-}C_5H_5)(CO)_2]$ (3)[a]

Fe–C(1)	1.725 (4)	C(8)–C(13)	1.391 (4)
Fe–C(2)	1.738 (4)	C(9)–C(10)	1.385 (5)
Fe–C(3)	2.083 (4)	C(10)–C(11)	1.365 (6)
Fe–C(4)	2.085 (4)	C(10)–H(10)	0.92 (5)
Fe–C(5)	2.088 (3)	C(11)–C(12)	1.358 (6)
Fe–C(6)	2.088 (4)	C(12)–C(13)	1.373 (5)
Fe–C(7)	2.081 (4)	C(14)–C(15)	1.387 (4)
Fe–B(4)	2.051 (3)	C(14)–C(19)	1.386 (4)
P–C(8)	1.825 (3)	C(15)–C(16)	1.381 (4)
P–C(14)	1.816 (3)	C(16)–C(17)	1.358 (5)
P–B(2)	1.898 (4)	C(17)–C(18)	1.372 (5)
P–B(3)	1.907 (3)	C(18)–C(19)	1.386 (5)
O(1)–C(1)	1.157 (4)	B(1)–B(2)	1.811 (4)
O(2)–C(2)	1.156 (4)	B(1)–B(3)	1.831 (5)
C(3)–C(4)	1.397 (5)	B(1)–B(4)	1.684 (5)
C(3)–C(7)	1.378 (6)	B(1)–B(5)	1.674 (5)
C(4)–C(5)	1.370 (6)	B(2)–B(5)	1.790 (5)
C(5)–C(6)	1.379 (6)	B(3)–B(4)	1.802 (5)
C(6)–C(7)	1.389 (6)	B(4)–B(5)	1.759 (5)
C(8)–C(9)	1.376 (4)	B(2)–B(3)	2.683 (5)

[a] The estimated standard deviations in the least significant figure are given in parentheses.

Table VII. Selected Dihedral Angles between Least-Squares Planes for $[(C_6H_5)_2PB_5H_7Fe(\eta^5\text{-}C_5H_5)(CO)_2]$ (3)[a]

plane	plane	angle, deg	plane	plane	angle, deg
2	1	22.46	5	3	84.70
3	1	125.63	5	4	116.10
3	2	148.07	6	1	129.24
4	1	101.19	6	2	132.25
4	2	115.20	6	3	54.89
4	3	51.90	6	4	106.01
5	1	65.29	6	5	64.37
5	2	76.19			

[a] Key: plane 1, B(2), B(3), B(4), B(5); plane 2, B(2), B(3), P; plane 3, B(1), B(2), B(3); plane 4, C(8), C(9), C(10), C(11), C(12), C(13); plane 5, C(14), C(15), C(16), C(17), C(18), C(19); plane 6, C(3), C(4), C(5), C(6), C(7).

Results and Discussion

The initial synthesis and ^{11}B NMR spectrum of $[(\mu\text{-}(C_6H_5)_2P)B_5H_8]$ (1) had been previously communicated from the reaction of $ClP(C_6H_5)_2$ with $Li[B_5H_8]$.[3] In our exploration of the synthesis and reaction chemistry of small heteroborane cluster systems, we have thoroughly characterized compound 1 spectroscopically and have studied its reaction and organometallic chemistry. The ^1H coupled and decoupled ^{11}B spectra for 1 are shown in Figure 1. The ^{11}B NMR spectrum previously reported by Burg[3] consisted of three sets of doublets, with the P–B coupling expected for the basal boron resonances nearest to the bridging phosphino group not observed. The failure to observe this P–B coupling is atypical of most bridged phosphinopentaborane systems.[1,4] It was suggested[3] that the reason for this observation was that the P–B coupling in $[(\mu\text{-}(C_6H_5)_2P)B_5H_8]$ was unusually small due to the phosphorus atom employing much of its s-electron character in bonding to the sp^2 orbitals of the substitutent phenyl groups. This would leave primarily the p orbital on the phosphorus for interaction with the basal boron atoms of the cage, resulting in a significantly reduced B–P coupling constant. In the ^{11}B spectrum that we observed for compound 1 (Figure 1), the P–B coupling was clearly resolved in the ^1H-decoupled spectrum into a doublet with a P–B coupling of 94 Hz. This value is consistent with the magnitude reported for other P–B couplings in bridged phosphinopentaborane systems (ranging from 77 to 111 Hz)[1] and in the Lewis acid–base adduct $(Me_3Si)_3P{\rightarrow}BH_3$ (92 Hz).[1] The ^1H-coupled ^{11}B spectrum showed a triplet centered at −22.7 ppm for the basal boron atoms bridged by the phosphino group (J_{PB} = 94 Hz and J_{BH} = 110 Hz), an upfield doublet at −45.6 ppm for the apical boron atom (J_{BH} = 153 Hz), and a downfield doublet at −0.5 ppm for the non-phosphorus-bridged basal boron atom set (J_{BH} = 164 Hz). The structure proposed for phosphinopentaborane compounds, based on both spectroscopic[1,3] and theoretical analyses,[2] consists of a modified pentaborane framework in which one of the bridging hydrogen atoms has been formally replaced by a bridging phosphino group. Since the phosphino group is believed to be a three-electron donor[1,6-8] and thus forms two two-center–two-electron bonds to the cage boron atoms, in contrast to the hydrogen atom's one-electron donation in a three-center–two-electron scheme, the basal B–B distance bridged by the phosphino group is expected to be significantly lengthened (from 1.86 Å in pentaborane(9) to 2.43–2.63 Å in phosphinopentaboranes[2]). This is in contrast to the proposed bonding in other main-group bridged pentaborane species, such as $[Cu(B_5H_8)(P(C_6H_5)_3)_2]$[26] and $[1\text{-}Br(\mu\text{-}(CH_3)_3Si)B_5H_7]$,[27] in which the bridging group simply acts as a "pseudohydrogen" atom and bonds to the cage through a three-center–two-electron bonding interaction. The bridging phosphorus atom is expected to be roughly tetrahedral ("quasitetrahedral")[27] in the phosphinopentaborane structure, which requires one phenyl group in 1 to be directed below the B_5 cage framework in an axial (or endo) fashion and the other phenyl group to be directed away from the cage in an equatorial (or exo) fashion. This expected axial–equatorial phenyl group orientation is confirmed in the ^{13}C NMR spectrum, in which the resonances for two chemically inequivalent phenyl groups are clearly distinguished. The resonances for the various carbon atoms of the phenyl rings were assigned by direct analogy with an analysis previously reported for $ClP(C_6H_5)_2$.[28]

The MNDO[2] calculated minimum energy geometry for compound 1 is shown in Figure 2. As described above, the minimum energy structure consists of a distorted square pyramid of boron atoms in which a basal B–H–B interaction has been replaced by a bridging $P(C_6H_5)_2$ group. The calculated B(2)–B(3) bond distance of 1.86 Å has opened to a B–B nonbonded distance of 2.44 Å, due primarily to the nature of the proposed two two-center–two-electron B–P–B bonding interactions. The phosphorus atom is calculated to be displaced from the B_4 basal plane of the

(26) Greenwood, N. N.; Howard, J. A.; McDonald, W. S. *J. Chem. Soc., Dalton Trans.* **1977**, 37.
(27) Calabrese, J. C.; Dahl, L. F. *J. Am. Chem. Soc.* **1971**, *93*, 6042.
(28) Wilke, C. A. *J. Mag. Reson.* **1979**, *33*, 127.

Scheme I. Deprotonation and Reaction Chemistry of Bridged (Diphenylphosphino)pentaborane

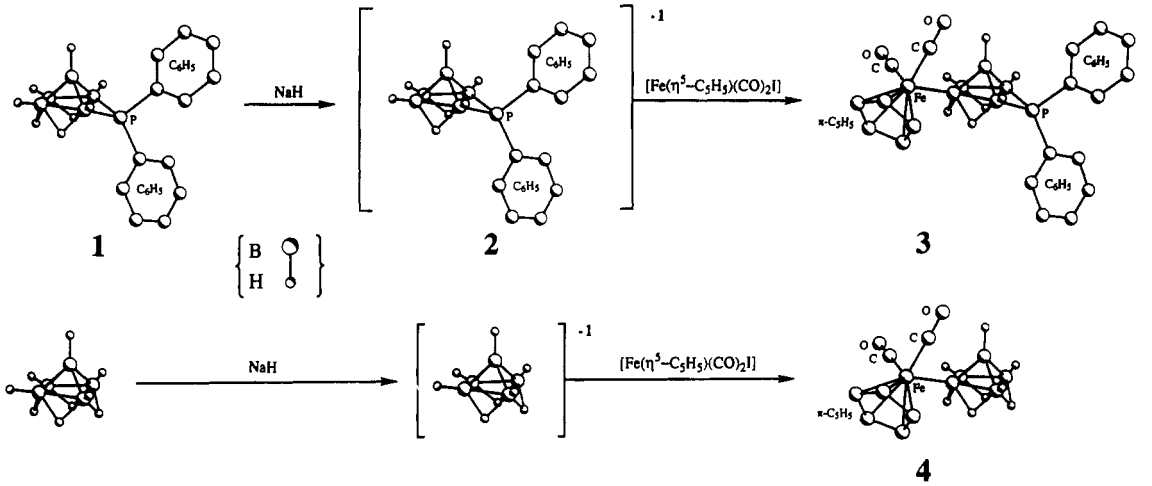

cage by 53.8° (as defined by the dihedral angle between the planes containing [B(2,3,4,5)] and [B(2,3)P]). Since each of the two B–P bonds can be best described as a two-electron–two-center interaction, the phosphorus atom is, as expected, approximately tetrahedral in its coordination to the two boron and two carbon atoms. The three highest occupied molecular orbitals primarily correspond to phenyl ring bonding orbitals. No orbitals corresponding primarily to a lone pair on phosphorus were found in the MO set. Indirect support for the involvement of the lone pair of electrons on the phosphorus in cage bonding is obtained from the failure of **1** to displace CH_3CN ligands from $[(CH_3CN)_3Mo(CO)_3]$, even under forcing conditions.

In the preparation of **1**, it appears that the lone pair of electrons on the phosphorus reactant is critically important for the spectroscopic observation or isolation of any phosphinopentaborane compound. It would be expected that if the lone pair were not essential, then the reaction of pentaborane(9) with $ClP(O)(C_6H_5)_2$, in which the phosphorus atom does not possess a lone pair of electrons, would be expected to form either a terminally substituted or a three-center–two-electron bridged pentaborane species. In the reaction of $ClP(O)(C_6H_5)_2$ with $Na[B_5H_8]$, no phosphorus substituted pentaborane compound was observed under any reaction conditions explored.

Compound **1** was readily deprotonated by the action of NaH to quantitatively yield the corresponding anion, **2** as a thermally stable solid. The ^{11}B NMR chemical shifts observed for **2** corresponded well with those previously reported in our work for the anion of $Na[B_5H_7(PRR')]$ (where R = $SiMe_3$ or H and R' = $C(OSiMe_3)(^tBu)H$).[2] In **2**, the B–P coupling (59.7 Hz) of the boron atoms bridged by the phosphino group was clearly resolved. The ^{13}C NMR spectrum once again showed the two chemically inequivalent phenyl groups of the phosphine clearly resolved into two assignable sets of resonances corresponding to the axial and equatorial phenyl groups, indicating the stereochemical rigidity of the phosphorus center on the NMR time scale. The upfield chemical shift in the ^{31}P spectrum for compound **2** relative to compound **1** indicates a relative shift of electron density from the cage to the phosphorus center, as expected.

The reaction of **2** with $[Fe(\eta^5\text{-}C_5H_5)(CO)_2I]$ produced the yellow $[((C_6H_5)_2P)B_5H_7(Fe(\eta^5\text{-}C_5H_5)(CO)_2)]$ complex (**3**) in high yield as an air-stable solid. This reaction is directly analogous to both the preparation of $[B_5H_8(Fe(\eta^5\text{-}C_5H_5)(CO)_2)]$ (**4**) from the reaction of $M[B_5H_8]$ (where M = Na or K) with $[Fe(\eta^5\text{-}C_5H_5)(CO)_2I]$, as reported independently by Gains[9] and Greenwood,[10] and also to the preparation of 6-$[B_{10}H_{13}(Fe(\eta^5\text{-}C_5H_5)(CO)_2)]$ (**5**) from the reaction of $[Fe(\eta^5\text{-}C_5H_5)(CO)_2I]$ with $B_{10}H_{13}^-$.[29a] A similar reaction of $[Fe(\eta^5\text{-}C_5H_5)(CO)_2I]$ with $Na[C_2B_4H_7]$ was found previously, however, to produce the iron-bridged metallacarborane species $[\mu\text{-}(Fe(\eta^5\text{-}C_5H_5)(CO)_2)C_2B_4H_7]$, rather that a terminally bound iron system.[29b] The ^{11}B NMR spectrum of **3**, shown in Figure 1, consists of five resonances at 23.3, 1.4, −23.6, −24.9, and −37.6 ppm in a 1:1:1:1:1 relative ratio. The resonance for the apical boron atom, at δ = −37.6 ppm, appears as a doublet in the ^1H-coupled spectrum. Of the four resonances assigned to the basal boron atoms, all appear as ^1H-coupled peaks except the resonance at +23.3. This latter downfield shifting of the coordinated basal boron resonance is consistent with metal coordination at a basal boron atom by replacement of a terminal hydrogen atom.[30-34] The magnitude of this downfield shift relative to pentaborane(9) is, however, unusually large and represents the largest downfield shift reported for an exo-substituted pentaborane species ($\Delta(\delta(\text{complex}) - \delta(B_5H_9))$ = +37.0 ppm).[9] This shift is considerably further downfield than either complex **4** (Δ = +21.9 ppm) or the related $[B_5H_8(Fe(\eta^5\text{-}C_5H_5)(CO)_2)_2]$ complex (Δ = +15.4 ppm).[10] This indicates that significant electron density has shifted from the basal-boron position to B(2), B(3), and the exopolyhedral substitutents of the cage system and that this electron density shift is clearly enhanced by the presence of the bridging phosphino group. The complex basal resonances at −23.6 and −24.9 ppm ^1H decouple to clearly show B–P coupled doublets. The only possible structure accounting for these data is a system in which the phosphino group is bridging at the B(2)–B(3) face and the iron unit attached to the cage in a terminal σ-bonded fashion at B(4). This structure for **3** is in contrast to the proposed product from the reaction of $[Fe(\eta^5\text{-}C_5H_5)(CO)_2(\text{cyclohexene})]$ and $[EB_{10}H_{12}]^-$ (where E = P or As) in which the iron atom is believed to be σ-bound directly to the heteroatom, $[B_{10}H_{12}E(Fe(\eta^5\text{-}C_5H_5)(CO)_2)]$.[35] The ^{31}P NMR resonance for **3** was observed at approximately the same chemical shift as for that of the free phosphinopentaborane compound (^{31}P for **1** = δ −52.3; ^{31}P for **3** = δ −50.4). This indicates that the electron distribution near the phosphorus is similar to that in the free phosphinopentaborane and that metal complexation does not occur at the phosphorus center. ^{13}C NMR data show, as for the other phosphinopentaborane species discussed here, that the two phenyl groups do not interconvert on the NMR time scale and can be clearly resolved.

The FT-IR spectrum of **3** shows two carbonyl stretches at 1990 ad 1934 cm^{-1} (Nujol). These values are slightly shifted to lower energy relative to the related pentaboranyl complex **4**, which has CO stretches at 2012 and 1956 cm^{-1} (CCl_4).[10] This indicates that the phosphinopentaboranyl cage is a slightly better electron-donating unit relative to the non-phosphaborane cage, although the

(29) (a) Sato, F.; Yamamoto, J. R.; Wilkinson, J. R.; Todd, L. J. *J. Organomet. Chem.* **1975**, *86*, 243. (b) Sneddon, L. G.; Beer, D. C.; Grimes, R. N. *J. Am. Chem. Soc.* **1973**, *95*, 6623.

(30) Gaines, D. F.; Walsh, J. L. *Inorg. Chem.* **1978**, *17*, 1238.
(31) Fischer, D. F.; Gaines, D. F. *Inorg. Chem.* **1979**, *18*, 3200.
(32) Weiss, R.; Grimes, R. N. *J. Am. Chem. Soc.* **1977**, *99*, 8087.
(33) Shore, S. G.; Ragaini, J. D.; Smith, R. L.; Cottrell, C. E.; Fehlner, T. P. *Inorg. Chem.* **1979**, *18*, 670.
(34) Wilcyznski, R.; Sneddon, L. G. *Inorg. Chem.* **1979**, *18*, 864.
(35) Yamamoto, T.; Todd, L. J. *J. Organomet. Chem.* **1974**, *67*, 75.

magnitude of the shift suggests that this is not a strong effect. This is supported by the observation by Greenwood that the replacement of a hydrogen atom on the cluster with the [Fe(η^5-C_5H_5)$(CO)_2$] units apparently has relatively little effect on the behavior of the cluster.[10] The B–H stretches for both complexes appear at approximately the same location (ν_{B-H}: **3** = 2576, **4** = 2575 cm^{-1}).

A single-crystal X-ray analysis confirms the general structural features proposed for **3** based upon spectral data. Bond angles, bond lengths, and interplane dihedral angles for **3** are given in Tables V–VII, respectively. The structure consists of a highly distorted square pyramid of boron atoms in which the B(2)–H–B(3) bond has been subrogated by a B–P–B bridge (Figures 3 and 4). The [Fe(η^5-C_5H_5)$(CO)_2$] unit is substituted for a terminal proton on B(4) with the (η^5-C_5H_5) ring directed below the basal-B_4 plane and the Fe atom 0.368 Å above this plane. The Fe–C(carbonyl) bond lengths are slightly shortened (average Fe–C = 1.731 Å) in comparison with other similar bond distances in iron carbonyl complexes (average Fe–$C_{(terminal)}$ ranging from approximately 1.74 to 1.82 Å),[36] as anticipated for **3** on the basis of IR data. The B(2)–B(3) atomic distance of 2.68 Å shows the structure to be based on an arachno 7-vertex parent species in which two adjacent verticies have been removed and the open face is bridged by the phosphino unit.[37] This can formally be thought of as derived from the two-electron reduction of a *nido*-pentaborane structure by the three-electron-donating phosphino unit to an *arachno*-pentaborane structure. On the basis of electron-counting schemes,[38] the structure is formally analogous to that of B_5H_{11}.[39,40] As anticipated, the observed B(2)–B(3) bond distance in **3** is much longer than that determined for B_5H_9 (gas phase structure, 1.811 ± 0.004 Å), but it is also significantly shorter than the analogous distance in B_5H_{11} (gas phase structure, 3.091 ± 0.010 Å).[40] This shortening is presumably due to the constraint on the bond distance imposed by the bridging phosphino group. The contrast between the bonding of the bridging phosphino group in **3** with those systems in which the bridging group is involved in a three-center–two-electron binding interaction is clearly evident by comparison of the bridged B(2)–B(3) atomic distances in **3** (2.68 Å) with structures such as [(μ-Be(η^5-C_5H_5))B_5H_8] (1.726 Å),[41] [(μ-Cu($P(C_6H_5)_3$)$_2$)B_5H_8] (1.70 Å),[26] [$(Fe(CO)_4B_7H_{12})^-$] (1.773 Å)[42], [1-Br(μ-$(CH_3)_3Si$)B_5H_7] (1.69 Å)[27] and [$Cu(P(C_6H_5)_3)_2B_5H_8Fe(CO)_3$] (1.663 Å).[43] The bridging phosphorus atom exhibits a distorted tetrahedral geometry in which the B(2)–P–B(3) bond angle has been reduced to 89.7° and the B(2,3)–P–$C_{equatorial}$ angle has been increased to an average of 122.1°. Other angles around the phosphorus are very close to tetrahedral. The variation in the bond angles around phosphorus is in agreement with those observed in $B_{10}H_{13}P(C_6H_5)_2$ in which the B–P–B angle was found to be 88.2° and the large angle to be close to 120°.[44] The phosphorus is located 0.516 Å below the least-squares basal-B_4 plane, which is a significantly smaller distance than the distances reported for the two-electron–three-center bridged metal systems (1.5–1.7 Å below the basal-B_4 plane).[43] The average B–P bond length of 1.90 Å is consistent with the other B–P bond lengths reported for the icosahedral phosphaboranes (1.90–2.05 Å).[2,6,44–50] The average P–C bond length of 1.821 is similar to that found in $P(C_6H_5)_3$ (1.829 Å), and the perpendicular orientation of the two phenyl groups on the phosphorus relative to the basal-B_4 plane is probably a consequence of crystal packing forces. The apical boron atom is not symmetrically bound to the four basal boron atoms, with long bonds to the phosphorus-bridged boron atoms (average B(1)–B(2,3) = 1.821 Å) and short bonds to the nonbridged boron atoms (average B(1)–B(4,5) = 1.679 Å). The high quality of the data set allowed the location of all of the hydrogen atoms on the phosphinopentaborane cage. The bridging hydrogen atoms of the cage were found to be asymmetrically bridged and shifted away from the iron center in each case (Δ(bond length) = 0.20 Å). Similar asymmetric hydrogen bridging has been reported for other systems,[2] including the iridium pentaboranyl complex [$(IrB_5H_8)(CO)(P(C_6H_5)_3)_2$].[51]

Acknowledgment. We wish to thank the National Science Foundation (Grant No. MSS-89-09793), the donors of the Petroleum Research Fund, administered by the American Chemical Society, the General Electric Co., the Rome Air Development Center (Award No. F30602-89-C-0113), IBM, and the Industrial Affiliates Program of the Center for Molecular Electronics for support of this work. We also wish to thank Mr. John A. Glass, Jr., for assistance with the MNDO calculations included in this work.

Supplementary Material Available: Tables of bond distances and angles, anisotropic thermal parameters, selected dihedral angles between least-squares planes, torsion angles, and all atom coordinates and isotropic thermal parameters including calculated, refined hydrogen atoms and ORTEP diagrams (21 pages); a listing of observed and calculated structure factors (22 pages). Ordering information is given on any current masthead page.

(36) Gress, M. E.; Jacobson, R. A. *Inorg. Chem.* **1973**, *12*, 1746.
(37) Rudolph, R. W. *Acc. Chem. Res.* **1976**, *9*, 446.
(38) Wade, K. *Adv. Inorg. Chem. Radiochem.* **1976**, *18*, 1.
(39) Lavine, L.; Lipscomb, W. N. *J. Phys. Chem.* **1954**, *22*, 614.
(40) Greatrex, R.; Greenwood, N. N.; Rankin, D. W. H.; Robertson, H. E. *Polyhedron* **1987**, *6*, 1849.
(41) Gaines, D. F.; Coleson, K. M.; Calabrese, J. C. *Inorg. Chem.* **1981**, *20*, 2185.
(42) Mangion, M.; Clayton, W. R.; Hollander, O.; Shore, S. G. *Inorg. Chem.* **1977**, *16*, 2110.
(43) Mangion, M.; Ragaini, J. D.; Schmitkons, T. A.; Shore, S. G. *J. Am. Chem. Soc.* **1979**, *101*, 754.
(44) Friedman, L. B.; Perry, S. L. *Inorg. Chem.* **1973**, *12*, 288.
(45) Todd, L. J.; Paul, I. C.; Little, J. L.; Welcker, P. S.; Peterson, C. R. *J. Am. Chem. Soc.* **1968**, *90*, 4489.
(46) Mastryukov, V. S.; Atavin, E. G.; Vilkov, L. V.; Golubinskii, A. V.; Kalinin, V. N.; Zhigareva, G. G.; Zakharkin, L. I. *J. Mol. Struct.* **1979**, *56*, 139.
(47) Wong, H. S.; Lipscomb, W. N. *Inorg. Chem.* **1975**, *14*, 1350.
(48) Getman, T. D.; Deng, H.-B.; Hsu, L.-Y.; Shore, S. G. *Inorg. Chem.* **1989**, *28*, 3612.
(49) Little, J. L.; Kester, J. G.; Huffman, J. C.; Todd, L. J. *Inorg. Chem.* **1989**, *28*, 1087.
(50) Thornton-Pett, M.; Beckett, M. A.; Kennedy, J. D. *J. Chem. Soc., Dalton Trans.* **1986**, 303.
(51) Greenwood, N. N.; Kennedy, J. D.; McDonald, W. S.; Reed, D.; Staves, J. *J. Chem. Soc., Dalton Trans.* **1979**, 117.